

# Effect of the Addition of Porcelain Tile Polishing Residue in Ceramic Masses for Sanitary Ware

Ricardo H. L. Silva<sup>a,b</sup>, Gelmires A. Neves<sup>b</sup> , Ana C. V. Nóbrega<sup>c</sup>, Rosiane M. C. Farias<sup>b</sup>,

Mônica F. B. Rocha<sup>d</sup>, Kleber G. B. Alves<sup>d\*</sup> , Romualdo R. Menezes<sup>b</sup> 

<sup>a</sup>Instituto Federal de Pernambuco, 55040-120, Caruaru, PE, Brasil.

<sup>b</sup>Universidade Federal de Campina Grande, Laboratório de Tecnologia de Materiais, 58429-900, Campina Grande, PB, Brasil.

<sup>c</sup>Universidade Federal do Rio Grande do Norte, Programa de Pós-graduação em Engenharia Civil e Ambiental, 59078-900, Natal, RN, Brasil.

<sup>d</sup>Universidade Federal de Pernambuco, Departamento de Engenharia Mecânica, 50670-901, Recife, PE, Brasil.

Received: December 15, 2022; Revised: August 16, 2023; Accepted: September 04, 2023

Currently, there is a severe shortage of good-quality feldspar deposits. On the other hand, porcelain tile polishing residue has been widely recognized as an alternative raw material for the ceramic industry. Thus, this research evaluated the effect of the partial replacement of feldspar by the porcelain polishing residue (PPR) in formulations for sanitary stoneware. It was replaced from 2% to 20% of the total mass of feldspar by the residue. The raw materials were characterized by X-ray fluorescence, X-ray diffraction, and particle size determination. Then, they were mixed in a wet ball mill, and the rheological properties of the suspensions were analyzed. Samples of the test were produced by slip casting and sintered at 1160 °C, 1180 °C, and 1200 °C. Rheological characteristics were not affected when up to 20% of feldspar was replaced by residue. Bodies with high amounts of PPR had flexural strength and water absorption values similar to those of bodies without PPR in formulations. Furthermore, apparent porosity values lower than the reference mass were obtained with the addition of 6% of the residue in the formulation.

**Keywords:** *Ceramic, sanitary stoneware, feldspar, porcelain tile polishing residue.*

## 1. Introduction

Porcelain tile is a ceramic building material with high mechanical strength, abrasion resistance, and excellent resistance to chemical attack. In Brazil, more than half of the total production of ceramic materials is for coatings, with a generation of 60,000 tons of porcelain tile polishing residue (PPR) per year<sup>1-3</sup>.

There are two types of porcelain tiles: polished and unpolished. The polished material, widely used due to its aesthetic appearance, undergoes a polishing process to improve the surface finish and shine the piece<sup>4,5</sup>. However, this step generates a huge amount of waste (PPR).

The PPR can be defined as a ceramic mixture resulting from the polishing step, containing material pulverized from the piece and the abrasive material released in this process, usually obtained in mud. After a drying, grinding, and sieving step, the residue appears as a white powder<sup>6</sup>.

The most used abrasive in the polishing step is composed of silicon carbide and cement based on magnesium oxychloride. During the polishing process, between 0.4 and 0.8 mm of porcelain material is normally removed from the tile surface to achieve the surface gloss level of 65 to 70%. This stage generates a large amount of waste from porcelain<sup>7,8</sup>. Generally, the waste contains about 1 to 5% by mass of silicon carbide (SiC) and 2 to 6% by mass of magnesium

oxychloride (MO) cement from the polishing tool<sup>9</sup>. Therefore, the polishing residue is composed of a mixture of abrasives and a high amount of ceramic coating<sup>6,10</sup>.

This type of waste contains silica (SiO<sub>2</sub>), aluminum oxide (Al<sub>2</sub>O<sub>3</sub>), and melting/fluxing oxides (K<sub>2</sub>O, Na<sub>2</sub>O, CaO, and MgO), which are similar to the composition of the ceramic material, indicating that the recycling of this material within the same process is a promising approach for the manufacture of traditional ceramic tiles<sup>11,12</sup>.

On the other hand, PPR must be used with caution due to the existence of silicon carbide (SiC). SiC decomposes and forms silica (SiO<sub>2</sub>) and carbon dioxide (CO<sub>2</sub>) at high firing temperatures (i.e., > 1000° C), and the generation of gas during the process can influence the characteristics of the final piece, such as the production of a porous microstructure<sup>11,13-21</sup>.

However, Bernarndin et al.<sup>22</sup> and Rambaldi et al.<sup>23</sup> analyzed the feasibility of using PPR to produce coatings by replacing sodium feldspar. As the sodium feldspar content was not high in the studied formulations, the waste utilization rate was relatively low, around 10%. Therefore, the new materials showed a significant decrease in the sintering temperature while maintaining the same properties as the original formulations. These results demonstrated that the recycling and exploitation of this type of waste can be viable for the ceramic industry.

\*e-mail: [kleber.gbvalves@ufpe.br](mailto:kleber.gbvalves@ufpe.br)

In this sense, researchers have analyzed the possible application of PPR as an alternative raw material for the sanitary ware industry<sup>9,23,24</sup>. They observed that it is possible to use PPR in partial replacement for feldspar in sanitary ware formulations. Additionally, the authors also observed that the use of PPR can increase the amount of mullite in the final piece<sup>25</sup>, and improve the pyroplastic deformation of ceramic materials. The microstructure of pieces produced with PPR also has phases related to the residue, such as silicon carbide, and periclase (MgO)<sup>24,26</sup>, which also contribute to changes in the properties of the sintered piece.

Despite the evaluation of the characteristics of sintered pieces observed in previously cited articles, the influence of PPR on the rheological characteristics of formulations suspensions is still not clear and the impact of the substitution of higher amounts of feldspar by PPR in sanitary ware bodies needs to be more understandable because of the kinetics of liquid phase formation, densification, and the crystallization process. Thus, this work aims to evaluate the effect of partial replacement of feldspar by porcelain tile residue in formulations for use in the manufacture of sanitary ware bodies.

## 2. Materials and Methods

### 2.1. Materials

For the development of this research, the following raw materials were used: kaolin (from Gaibú-PE), ball clay (from Itambé-PB), quartz (from Parelhas-RN), feldspar (from Parelhas-RN), and residue from porcelain tile polishing - PPR.

The raw materials used in this study presented a granulometry smaller than the No. 200 sieve (0.074 mm). The materials were characterized by X-ray fluorescence (Shimadzu, XRF 720), X-ray diffraction (Shimadzu, XRD 6000), with  $\text{CuK}\alpha$  radiation (40kV/30mA) and goniometer speed of 2 °/min and step of 0.02°, with a sweep from 5° to 60°; differential thermal analysis (DTA) and thermogravimetric (TG) were carried out under air atmosphere, with a heating rate of 10 °C/min (Shimadzu, DTG-60H) and granulometric analysis by laser diffraction (Cilas, 1064 LD).

### 2.2. Methodology

The samples were formulated to replace the feldspar content by 0% (M0), 2% (PPR2), 6% (PPR6), 10% (PPR10), and 20% (PPR20) of porcelain tile polishing residue. These percentages are related to the total mass of feldspar. The formulations used are presented in Table 1. The reference mass (M0) was chosen based on the formulation of a commercial mass for the production of sanitary ware and also according to guidelines in the literature<sup>27</sup>.

The raw materials were dispersed via aqueous ball milling process. An amount of 29 wt% of solid was used in the dispersion process and the rotational speed was set to 70 rpm, 65% of the critical velocity of the mill. Sodium silicate (Pernambuco Química S/A), 0.6 wt%, was used as dispersant additive. The process was carried out for 1.5h. Then, the dispersions were poured in plaster mounds, by a slip casting process. Samples of 60 mm x 20 mm x 5 mm were produced. Then, specimens were dried in air (at room temperature) for 24h and after in an oven for 24 hours at 100 °C.

The rheological characterization of the dispersions was first determined by the deflocculation curves of all the prepared masses. To obtain these curves, the action of sodium silicate (Pernambuco Química S/A) was analyzed by the behavior of the apparent viscosity of the suspension as a function of the addition of the deflocculant. The amount of deflocculant (volume (ml) per 100 g/dry mass) was increased, and apparent viscosity was determined<sup>28,29</sup>. Viscosity was determined with a Brookfield model RVT viscometer (rotation speed of 20 rpm and “Spindel” no. 2).

In determining the rheological characteristics, suspensions that obtained curves of maximum deflocculation were used to determine drying time (DT), setting rate (SR), body moisture, evaluate the detachment of the body from the mold, and  $\alpha$  ratio. SR is defined as the mass in grams of the wet film of the slip, deposited in 5 minutes in a gypsum stamp (mold) in the shape of a spherical cap with a capacity of about 200 ml<sup>27</sup>. To determine it, a gypsum mold made in the laboratory was used with the same porosity characteristics as molds used commercially for the production of sanitary ware, i.e., a volume of 1000 ml and a dwell time of 2 minutes, after which the plaster stamp was drained. These conditions are indicated in the literature<sup>27</sup> for industrial masses. Then, DT was determined, which is the time required for the surface deposited on the stamp, after draining, to lose its specular shine and become matte.

The body detachment characteristic was evaluated by estimating the greater or lesser ease with which the piece used to measure SR and DT can be detached from the plaster stamp<sup>27</sup>. Body moisture was determined by the percentage of water retained in the piece after measuring the DT, expressed as a percentage of water in the wet body. The alpha ratio is determined by the quotient between the times (in seconds) to drain (in the Mariotte viscometer) the volumes of 200 and 250 ml of slip<sup>27</sup>.

Shrinkage and sintering behavior were evaluated with a dilatometry test (Seratam, TMA Setsys 16/18). Then, specimens were dried in the air for 24 h, followed by drying in an oven at 110 °C for 24 h. The specimens were sintered at 1160 °C, 1180 °C, and 1200 °C. The following firing cycle was used: room temperature to 600 °C with 3 °C/min;

**Table 1.** Composition of the ceramic masses used.

Formulation	Ceramic mass (%)				
	Kaolin	Ball clay	Quartz	Feldspar	PPR
M0	26.8	19.6	6.4	47.2	0.0
PPR2	26.8	19.6	6.4	46.3	0.9
PPR6	26.8	19.6	6.4	44.4	2.8
PPR10	26.8	19.6	6.4	42.5	4.7
PPR20	26.8	19.6	6.4	37.8	9.4

up to 1000 °C with 5 °C/min; and up to the final temperature with 2 °C/min. The dwell time is 60 minutes at the final<sup>30,31</sup>. The bodies were cooled overnight inside the furnace.

The sintered specimens were also characterized by X-ray diffraction (Shimadzu, XRD 6000) and scanning electron microscopy (Shimadzu, SEM SSX-550).

The water absorption<sup>32</sup>, linear drying shrinkage<sup>33</sup>, linear firing retraction<sup>33</sup>, apparent porosity<sup>34</sup>, and flexural strength at three points (modulus of rupture)<sup>35</sup> (Shimadzu, Autograph AG-X, load application speed of 0.5 mm/min) were determined. Statistical analysis was performed using the t-test for means and the F-test for variance evaluation.

### 3. Results and Discussion

The chemical compositions of the raw materials used are listed in Table 2. It should be noted that ball clay and kaolin presented percentages of 50.8 and 48.3% of silicon oxide (SiO<sub>2</sub>), respectively. Silica comes from the free quartz present in the samples and from kaolinite and illite clay minerals. The Al<sub>2</sub>O<sub>3</sub> contents were 29.5% for ball clay and 38.2% for kaolin and are related to the octahedral layer of kaolinite clay mineral and mica<sup>36</sup>. Fe<sub>2</sub>O<sub>3</sub> contents of 3.0% for ball clay and 2.3% for kaolin are within the acceptable limit to produce sanitary ware due to the requirements in the manufacture of light-colored artifacts<sup>37</sup>.

Alkaline oxides are the source of the melt that feldspar provides in the ceramic mass. A percentage of these oxides around 10% (Na<sub>2</sub>O+K<sub>2</sub>O) is observed in Table 2, typical of feldspars used for sanitary stoneware<sup>38-40</sup>, which can be classified as a potassium-sodium feldspar.

Evaluating the chemical composition of PPR, it is observed that its contents are similar those of porcelain polishing residue used in the literature by Bernardin et al.<sup>22</sup>, Rambaldi et al.<sup>23</sup> and Ke et al.<sup>24</sup>. The PPR has high levels of CaO and MgO, which are alkaline earth fluxes, which are related to the development of high levels of liquid phase during ceramic processing and cause the porcelain tile polishing residue to increase melting potential<sup>24</sup>. Regarding iron oxide (Fe<sub>2</sub>O<sub>3</sub>), the percentage of 0.6% indicates that the products of the firing of this raw material will probably present light colors, according to the literature<sup>24</sup>.

The X-ray diffractogram of the feldspar (Figure 1) shows characteristic peaks of sanidine - potassium-sodium feldspar (JCPDS 10-0357), quartz (JCPDS 46-1045) and muscovite mica (JCPDS 83-1803). For PPR, the crystalline phases presented are quartz (JCPDS 46-1045), cristobalite (JCPDS 82-0512), mullite (JCPDS 83-1881), and silicon carbide (JCPDS 89-2640). XRD patterns comprising PPR

with traces of silicon carbide and quartz are common in the literature<sup>24,26</sup>. XRD of kaolin and ball clay shows the presence of kaolinite (JCPDS 89-6538) and quartz (JCPDS 46-1045) as crystalline phases. Ball clay also presents peaks of smectite (JCPDS 10-0357) and feldspar (JCPDS 84-0710). These results are in line with those found in the literature focused on the characterization of kaolin and ball clay<sup>41-43</sup>.

Table 3 displays the values of the accumulated granulometric fractions below 2 µm, between 2 and 20 µm and greater than 20 µm, as well as the values of the mean diameter of the particles. The feldspar used in the formulation had a mean particle diameter (27.03 µm) greater than that of the PPR used in this study (6.78 µm). PPR has a higher number of fine particles, with a higher fraction accumulated in the ranges with a diameter of less than 2 µm and a diameter between 2 µm and 20 µm.

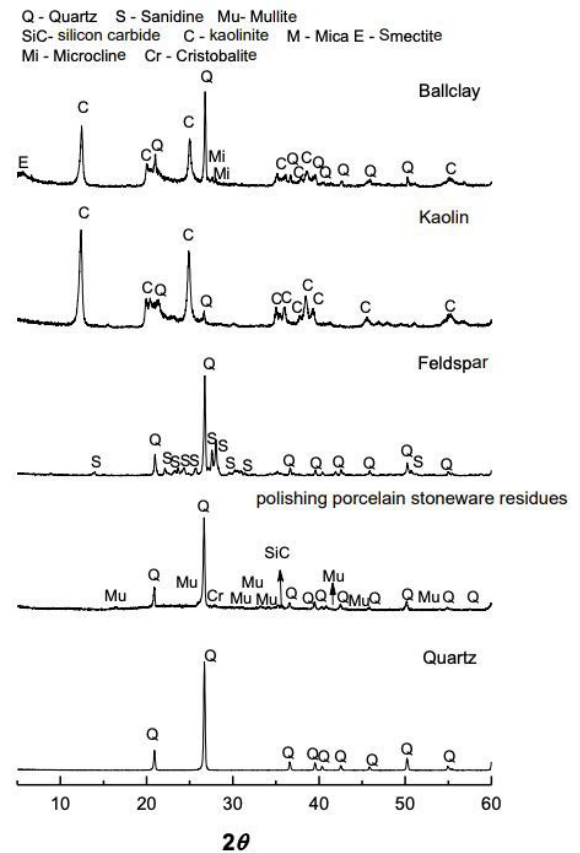


Figure 1. XRD curves of the raw materials.

Table 2. Chemical composition of the raw materials.

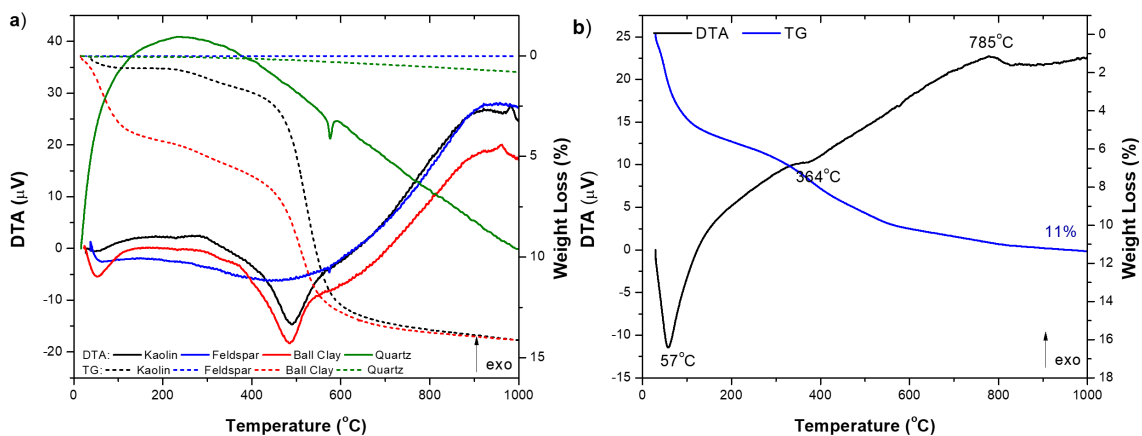
Raw materials	Oxides (%)									
	SiO <sub>2</sub>	Al <sub>2</sub> O <sub>3</sub>	Fe <sub>2</sub> O <sub>3</sub>	TiO <sub>2</sub>	CaO	MgO	Na <sub>2</sub> O	K <sub>2</sub> O	Other	LOI <sup>b</sup>
Ball clay	50.8	29.5	3.0	0.6	0.2	1.2	ND <sup>a</sup>	1.1	0.5	13.1
Kaolin	48.3	38.2	2.3	0.4	0.2	0.3	ND <sup>a</sup>	ND <sup>a</sup>	0.2	10.1
Quartz	96.8	2.3	0.1	ND <sup>a</sup>	0.1	ND <sup>a</sup>	ND <sup>a</sup>	0.1	0.3	0.3
Feldspar	72.3	16.2	0.2	ND <sup>a</sup>	0.4	ND <sup>a</sup>	3.2	6.8	0.3	0.6
PPR	62.6	18.9	0.6	0.2	1.4	10.3	ND <sup>a</sup>	2.1	1.2	2.7

<sup>a</sup>ND – Not detected; <sup>b</sup>LOI – Loss on ignition

**Table 3.** Particle size fractions.

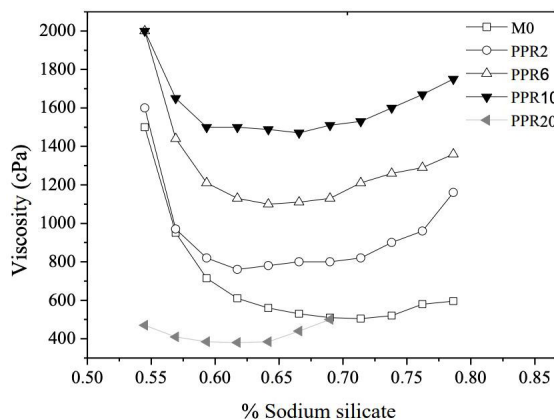
Samples	( $x \leq 2 \mu\text{m}$ ) (%)	( $2 \mu\text{m} < x \leq 20 \mu\text{m}$ ) (%)	( $x > 20 \mu\text{m}$ ) (%)	Mean diameter ( $\mu\text{m}$ )
Kaolin	44.4	55.6	0.0	3.3
Ball clay	37.7	56.2	6.1	5.6
Quartz	18.8	58.9	22.3	12.2
Feldspar	6.1	37.8	56.1	27.0
PPR	24.4	70.0	5.6	6.8

x = accumulated fraction.

**Figure 2.** Thermogravimetric and thermodifferential curves of the raw materials (a) and PPR (b).

The greater fineness of the PPR used stands out due to the high content of particles with dimensions lower than  $2 \mu\text{m}$ , which indicates that the reactivity of the PPR is very high. This may favor the processes of densification of the specimens produced at lower temperatures, since smaller particle sizes and larger surface areas are important factors for increasing reactivity between particles, accelerating reaction kinetics, and favoring the diffusion process that dictates phase transformations. However, the difference in the granulometric distribution of the PPR can compromise the packing of the system. In this case, even with a high content of fine particles, there may be a decrease in the densification of the system and/or an increase in the linear firing shrinkage due to the use of porcelain tile polishing residue<sup>44</sup>.

Figure 2 depicts the thermogravimetric and thermodifferential curves (TG and DTA) of the raw materials (Figure 2a) and PPR (Figure 2b). Kaolin DTA exhibits an endothermic peak at approximately  $491 \text{ }^\circ\text{C}$ , characterized by the loss of hydroxyls, and an exothermic peak with a maximum at  $981 \text{ }^\circ\text{C}$ , possibly characteristic of mullite nucleation. In addition, the Ball Clay shows an endothermic peak at  $53 \text{ }^\circ\text{C}$ , characteristic of the presence of adsorbed free water, and an endothermic peak at approximately  $484 \text{ }^\circ\text{C}$ , attributed to the presence of hydroxyls, and an exothermic peak with a maximum at  $959 \text{ }^\circ\text{C}$ , characteristic of mullite nucleation. In turn, analyzing the DTA curve of feldspar and Quartz, endothermic peaks were observed at  $574 \text{ }^\circ\text{C}$  and  $573 \text{ }^\circ\text{C}$ , respectively, describing the polymorphic transformation of  $\alpha$  (alpha) quartz into  $\beta$  quartz (beta)<sup>27</sup>. The DTA curve of the PPR (Figure 2b) shows an endothermic peak at  $57 \text{ }^\circ\text{C}$ ,

**Figure 3.** Deflocculation curve of the ceramic mass.

characteristic of the presence of adsorbed free water; an endothermic peak at approximately  $364 \text{ }^\circ\text{C}$ , which may be related to structural water loss from the material originating from the cementitious matrix of the abrasive (magnesium oxychloride cement); and an exothermic peak with a maximum at  $785 \text{ }^\circ\text{C}$ , which may be related to the burning and decomposition of silicon carbide.

Figure 3 illustrates the deflocculation curves of the analyzed formulations. It is observed that the addition of the PPR caused an increase in the viscosity of the dispersions, probably due to the higher content of fine particles and/or a contribution to the zeta potential of the Ca and Mg presented in the PPR.

However, this second approach is less significant than the first because the Ca and Mg present in PPR are present in the cement matrix of the material and are not easily exchanged with the medium. Thus, their release into the environment must be slow, influencing the zeta potential of the particles in the medium less intensely. Thus, compared to the short period of paste preparation and viscosity determination, the influence of the fine content is more significant. It is also verified that, as the level of PPR increases, there is a shift in the point of minimum viscosity for higher levels of deflocculants. This is associated with the need for a greater amount of stabilizing agent in the system because of the higher amount of fines and consequently the higher surface area in the system<sup>44</sup>.

As observed in Table 4, the formulations containing PPR have slip densities similar to the values of the M0 formulation. Formulation with up to 6% of waste have  $\alpha$  ratios similar to the reference formulation. These results are in line with those presented by Souza Santos<sup>27</sup> for formulations aimed at application in the manufacture of sanitary ware

Based on the values obtained for SR and DT of the formulations, it is not possible to visualize the influence and/or trends of the PPR on the setting behavior of the formulation. This is reinforced by the similar  $\alpha$  ratio and body moisture values of all analyzed formulations. Thus, it appears that the addition of PPR in the partial replacement of feldspar, in the range of values used in this study, does not cause significant changes in the technical characteristics of the dispersions produced.

Figure 4 shows the dilatometry curves of M0, PPR6, PPR10, and PPR20 samples. The curves show the shrinkage associated with the dehydroxylation of clay minerals, starting at approximately 520 °C. At 573 °C, the dimensional variation is related to the expansion of the polymorphic transformation of the alpha quartz into beta. During the sintering, the feldspar melting starts at around 1050 °C, which promotes the development of a more liquid phase in the system  $K_2O-Na_2O-SiO_2$ . The phenomenon causes densification and shrinkage of the body. In the reference composition, the higher firing shrinkage occurred at 1187 °C. However, with the rise in the PPR amount and the MgO content, this temperature decreased. The presence of alkaline-earth oxide, such as MgO, and alkaline oxides causes a synergistic effect on the melting potential of the fluxing material used, and the developed liquid phase begins to flow at lower temperatures. Moreover, the viscosity of the liquid phase containing both types of oxides decreases and the dissolution of silica increases with the introduction of alkali earth oxides, which also supports the decrease in the beginning of the sintering temperature. This decrease in

the sintering temperature was observed in the samples with 6% and 10% of the feldspar replaced by PPR (Figure 4). However, in the samples with 20% substitution this tendency was not observed. The temperature of maximum shrinkage of the sample with 20% was lower than those of the reference sample but higher than those of the 6 and 10% samples. Furthermore, the amount of shrinkage decreased. This could be related to the decomposition of SiC and the formation of a high amount of  $CO_2$  and  $SiO_2$ . The  $SiO_2$  formed and the gas present in the liquid phase increase the viscosity and difficulty of the flow and the mechanism of liquid-phase densification.  $CO_2$  also decreases the shrinkage of the body. Because of this, the composition with 20% feldspar replacement could have higher porosity and lower strength than the other compositions. The curves also show the shrinkage related to the formation of mullite, with onset varying from 886 °C to 940 °C, and the shrinkage associated with the major process of densification, with the formation of the liquid phase and the development of other crystalline phases<sup>44</sup>.

The addition of the PPR accelerated the mullite nucleation process (Figure 4), probably due to the precocious development of liquid phases. It also caused a decrease in the temperature of maximum shrinkage (densification), which was from 1187 °C in the reference sample (M0) to 1167 °C in the sample with 10% of porcelain polishing residue (PPR10). This behavior is interesting because it indicates that by increasing the residue content of porcelain tile polishing (up to 20%), it is possible to reduce the optimal sintering temperature without an exaggerated rise in firing shrinkage and, consequently, there is no greater tendency or possibility to change the format of the final piece.

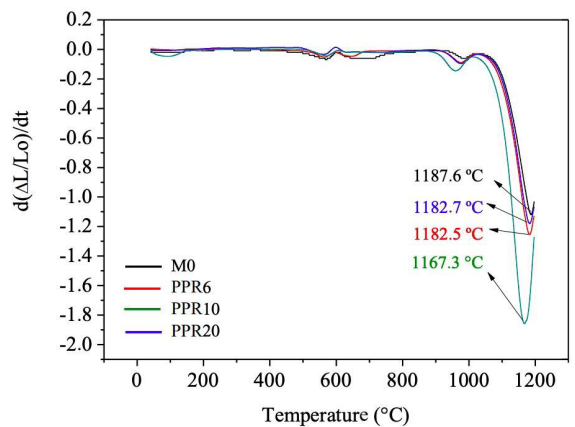


Figure 4. Dilatometric curve of the ceramic mass.

Table 4. Rheological properties of the ceramic formulations.

Properties	M0	PPR2	PPR6	PPR10	PPR20
Specific mass ( $g/cm^3$ )	1.76	1.75	1.74	1.75	1.74
Setting rate – SR (g)	56.5	57.0	56.5	69.4	78.0
Drying time – DT (s)	76.0	66.4	70.0	82.9	71.5
$\alpha$ ratio	0.62	0.60	0.62	45.87	0.52
Body moisture (%)	26.8	20.4	26.8	29.7	33.1
Detachment evaluation	Good	Good	Good	Good	Good

The X-ray diffractograms of the samples after the sintering process are shown in Figure 5. The mineralogical phases can be observed in all samples: mullite (JCPDS 79-1276), quartz (JCPDS 46-1045), and cristobalite (JCPDS 82-0512), with a predominance of mullite peaks in the diffractograms. There was no significant change in the phases formed after sintering at the evaluated temperatures (Figure 5).

As the presence of crystalline phases associated with Mg is not observed, it is believed that magnesium oxide dissolved in the liquid phase during firing and remained in the glass phase after cooling. This may be related to the fact that the total MgO content in the analyzed formulations, even in those with the addition of 20% of PPR, was less than 3%, making it difficult to precipitate cordierite, and also because of the  $\text{SiO}_2\text{-Al}_2\text{O}_3\text{-MgO}$  system, the formation of cordierite (considering the compositions of the masses used) only occurs at temperatures above 1400 °C.

Figure 6 shows SEM images (of fracture surfaces) of the formulations M0, PPR6, PPR10, and PPR20 after heat treatment at 1160 °C and 1200 °C. Heat treatment provided a microstructure characterized by the presence of small needles of mullite crystals and quartz grains. In PPR20 samples (Figures 6g and 6h), there was the development of more columnar and not so acicular mullite crystals, indicating growth kinetics of this material different from those that occur in the M0 sample (Figures 6a and 6b).

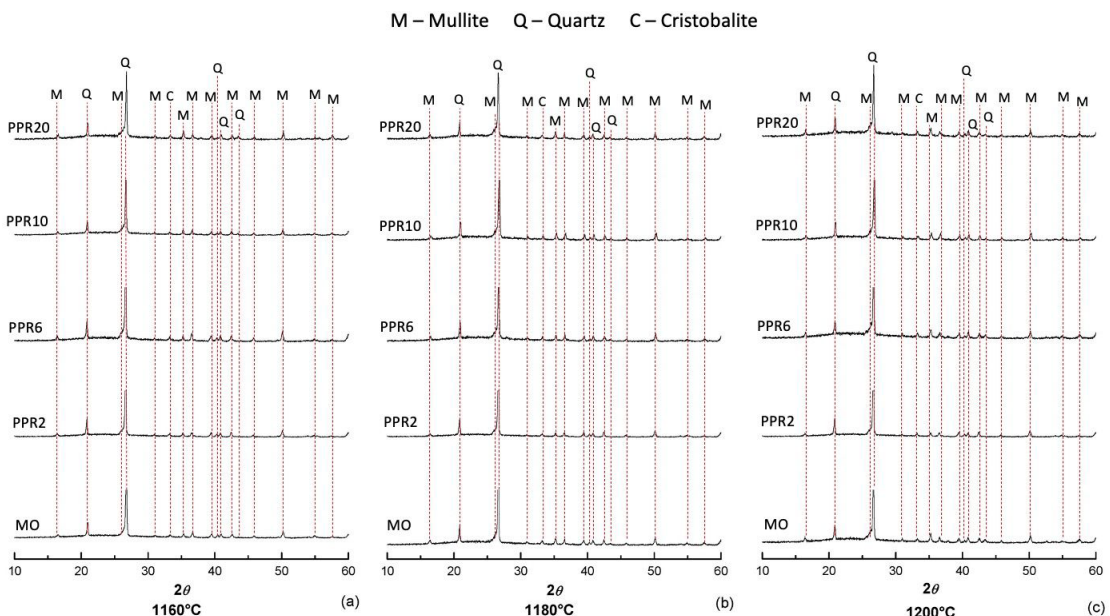
Figures 7a and 7b show the mean values obtained for the linear drying shrinkage and linear firing shrinkage of the studied formulations. It is observed that the samples containing PPR do not show statistically significant differences in drying shrinkage (t-test, p-value > 0.05). However, it is observed that there is an increase in the linear drying shrinkage with the standard mass (t-test, p-value < 0.05). This may be associated with a decrease in the packing of the system when the PPR is added, considering that it has a particle size distribution

with a smaller average particle size and a higher fraction of fines than feldspar.

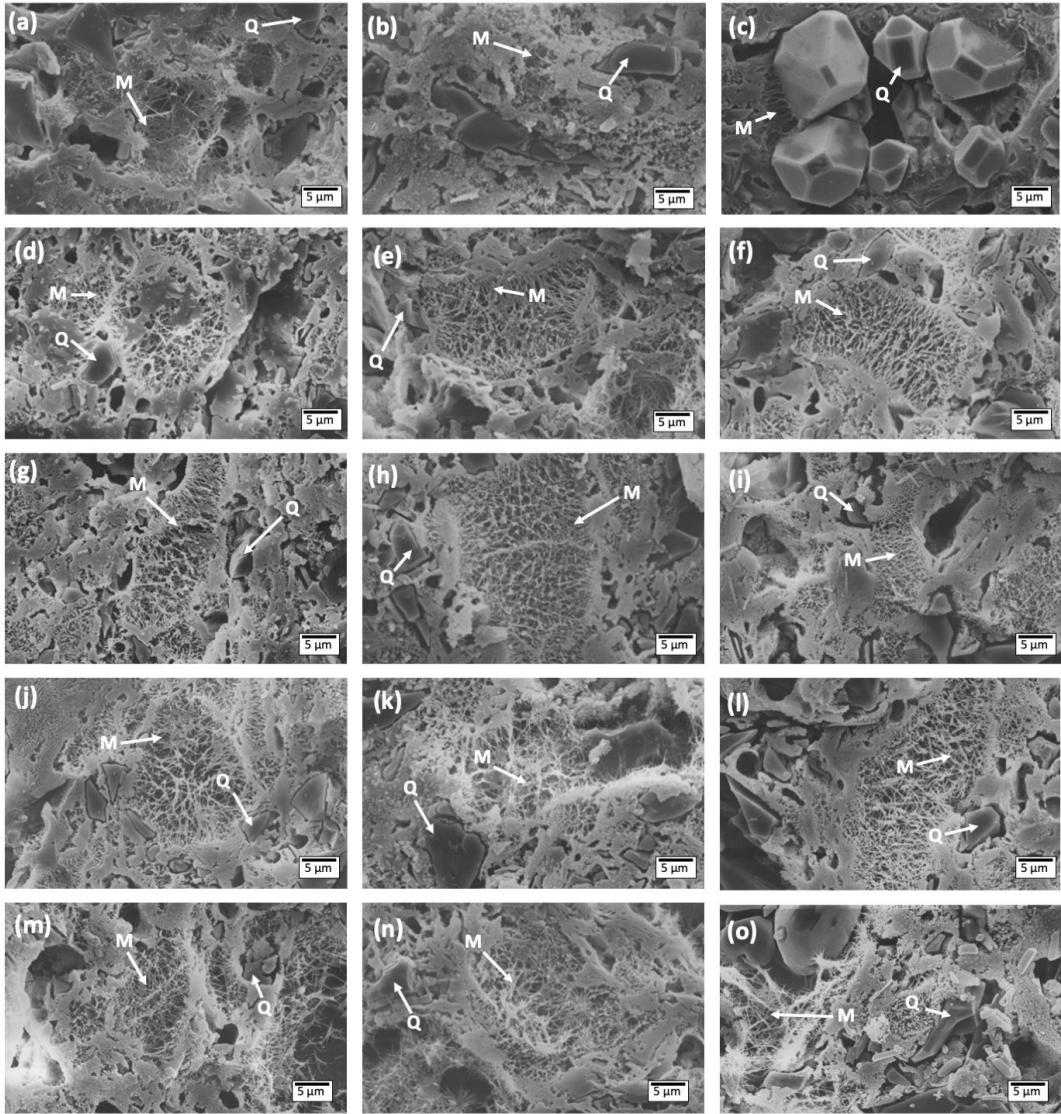
All analyzed samples show linear firing shrinkage of less than 11%, which follows data from the literature<sup>45-47</sup> for porcelains with a high amount of vitreous phase or sanitary ware, which shows linear firing shrinkage values around 10%. The reference mass showed the expected behavior of rising linear shrinkage with the firing temperature (t-test, p-value < 0.05). For samples containing PPR, linear shrinkage initially increases, reaches a maximum value at 1160 °C, and then decreases with increasing firing temperature. At 1200 °C, linear shrinkage drops below 8.0%, implying that PPR samples produce some volume expansion. This shrinkage phenomenon may be occurring because of two superimposed processes: a possible expansion due to the production of gases inside the piece and a large amount of glass phase, which together may imply a lower final firing shrinkage. It is probably related to the fact that the SiC particles decompose and form  $\text{SiO}_2$  and  $\text{CO}_2$  at high firing temperatures<sup>11,24</sup>.

Figure 8a presents the water absorption, and Figure 8b shows the apparent porosity values of the analyzed samples. The percentages of absorption initially decrease at 1160 °C and 1180 °C, then maintain a lower value of around 1.5% at 1160 °C and 1.15% at 1180 °C. Water absorption increases when the sintering temperature reaches 1200 °C. This behavior can be attributed to the formation of open pores on the surface of the sample, due to the decomposition of SiC into  $\text{SiO}_2$  and  $\text{CO}_2$ <sup>24</sup>.

The Brazilian standard for sanitary ware<sup>32</sup> establishes water absorption values of less than 0.5% for the application of ceramics such as sanitary stoneware. Thus, it appears that the reference mass and PPR2 are within the threshold of the standard after firing at 1200 °C, while the other samples containing 6%, 10%, and 20% of PPR have values above the norm after firing at 1160 °C, 1180 °C, and 1200 °C.



**Figure 5.** XRD curves of the ceramic mass as a function of the partial substitution of feldspar by PPR at the sintering temperatures of (a) 1160 °C, (b) 1180 °C, and (c) 1200 °C.



**Figure 6.** SEM micrographs of samples at: 1160 °C (a) M0, (d) PPR2, (g) PPR6, (j) PPR10, (m) PPR20; 1180 °C (b) M0, (e) PPR2, (h) PPR6, (k) PPR10, (n) PPR20; and 1200 °C (c) M0, (f) PPR2, (i) PPR6, (l) PPR10, (o) PPR20. (M = mullite, Q = Quartz).

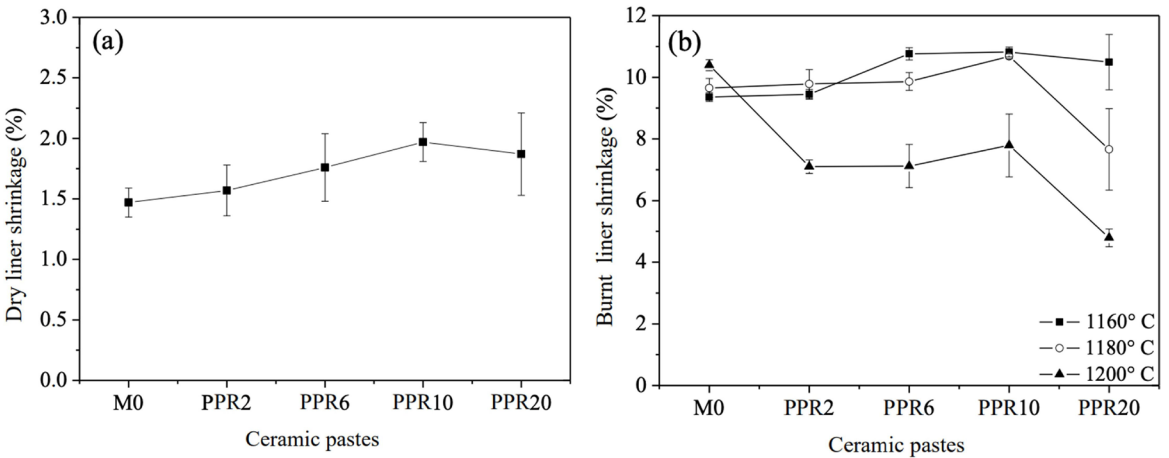


**Figure 7.** Linear drying shrinkage(a) and linear firing shrinkage (b).

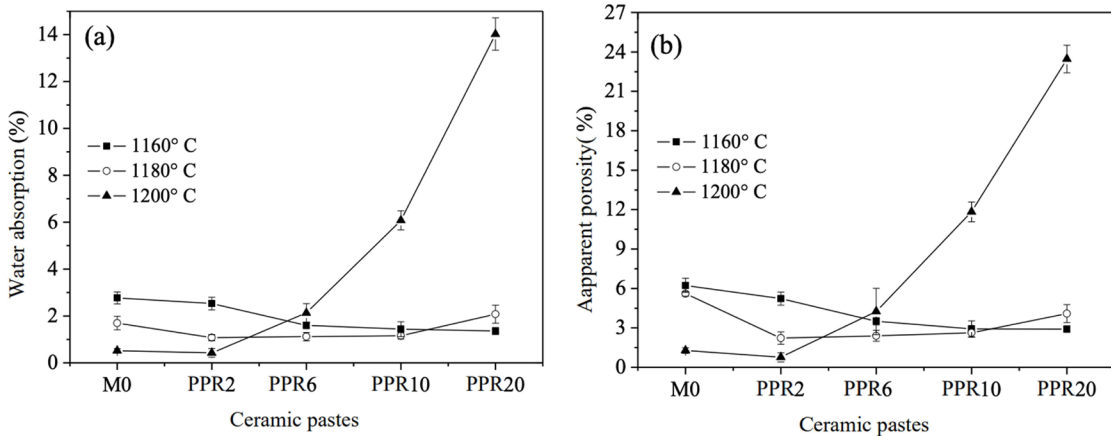


**Figure 8.** Water absorption (a) and apparent porosity (b) in the function of the partial substitution of feldspar by PPR at the sintering temperatures of 1160 °C, 1180 °C, and 1200 °C.

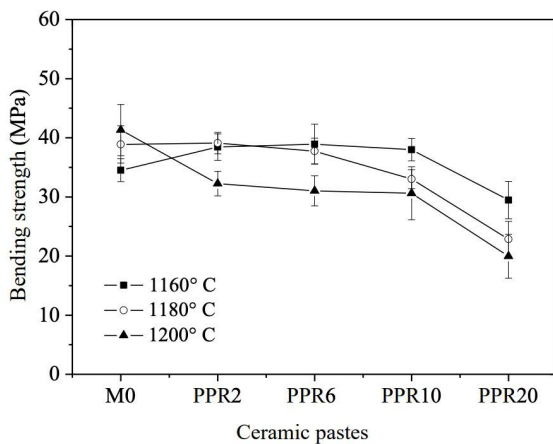


**Figure 9.** Flexural rupture strength in the function of the partial substitution of feldspar by PPR at the sintering temperatures of 1160 °C, 1180 °C, and 1200 °C.

This effectively restricts the amount of waste that can be recycled in compositions for sanitary stoneware to 2% of the partial replacement of feldspar by waste from porcelain tile polishing.

The apparent porosity of the samples containing PPR and fired at 1160 and 1180 °C did not change from the values obtained for bodies produced with the reference formulation (test  $t$ ,  $p < 0.001$ ). However, when sintering temperature increases to 1200 °C samples with more than 6% had apparent porosity higher than reference sample (test  $t$ ,  $p < 0.001$ ). SiC decomposes into silica and CO<sub>2</sub> during the sintering, and this gas could increase the porosity of the samples, according to the amount of SiC present and to the quantity of liquid phase generated during sintering. Results indicated that at lower temperatures, such as 1160 and 1180 °C, apparently a small oxidation of the SiC occur, which did not increase the porosity. However, at 1200 °C samples with amounts of PPR higher than 6% presented a significant increase in apparent porosity compared to bodies produced with the reference formulation (test  $t$ ,  $p < 0.001$ ).

Because of this phenomenon, studies<sup>12-15</sup> indicate that PPR should be avoided in ceramic masses at the risk of generating porous materials when fired at temperatures above 1000 °C. However, the results (Figure 8) indicated that up to 2% of residue can be used without changing the apparent porosity of the piece.

The flexural strength of the analyzed samples is shown in Figure 9. Most samples showed resistance values greater than or equal to 30 MPa, except for sample PPR20 at 1180 °C and 1200 °C. The reference sample has a maximum value of 41 MPa after firing at 1200 °C. It is observed that the flexural strength decreases with increasing firing temperature for samples PPR2, PPR6, PPR10, and PPR20. However, for samples PPR6 and PPR10, these values remain equal (38.00 MPa) with the test specimens of the reference mass at a sintering temperature of 1180 °C. The mechanical behavior is correlated with the sintering behavior, the formation of SiO<sub>2</sub> and CO<sub>2</sub> at high firing temperatures, and the consequent development of porosity in samples<sup>11,24</sup>. Flexural strength initially increases and reaches the maximum value (39.10 MPa) for sample PPR2 at 1180 °C. The highest value observed was for the reference sample (M0), which was above the value of 40 MPa.

The relation between the water absorption and the strength of the produced bodies (Figure 7 and Figure 8) is intimately associated with the densification and the shrinkage performance of the developed compositions, observed in Figure 3. With the rise in PPR content, the MgO improved the densification process and reduced the required sintering temperature up to 6% feldspar replacement. This are intimately related with the synergistic effect due to the presence of alkaline and alkaline earth oxides in the body in the appropriated amount. However, when the amount of PPR increased, the generation of CO<sub>2</sub> also raised, and at low temperature, such as 1160 °C, occur a decrease in flexural strength. With the rise in the firing temperature, the flexural strength continued low. The increase in the temperature up to 1200 °C improve the overall densification with the development of higher amount of liquid phase and decreasing the water absorption. However, the presence of high amount of CO<sub>2</sub> are intimately related with a higher content of closed porosity, and this causes a decrease in the flexural strength.

Figure 3 indicates through the decrease in the amount of shrinkage of the composition with 20% of feldspar replacement the presence of those pores caused by the entrapped gas. Thus, for an efficient incorporation of PPR in porcelain sanitary ware formulation low amount of residue must be used, but this process can be an efficient method to use this waste in the porcelain sanitary ware production cycle.

No statistically significant differences in the flexural strength values in the samples PPR2, PPR6, and PPR10 were observed with the increase in the firing temperature from 1160 °C to 1180 °C (t-test, p-value > 0.05). The PPR20 formulation showed lower flexural strength, consistent with the water absorption results. This behavior was probably due to the higher porosity.

#### 4. Conclusions

The rheological and detachment characteristics of the evaluated formulations were not impaired when partial replacement of feldspar by the residue from porcelain tile polishing in up to 20% in the ceramic mass. The use of porcelain tile polishing residue leads to the development of a microstructure with the same characteristics as a traditional triaxial ceramic mass. Specimens produced with formulations containing porcelain tile polishing residue have lower flexural strength values and reduced water absorption and apparent porosity. The content of porcelain tile polishing residue in the formulations influences the densification behavior. Masses with up to 2% of porcelain tile polishing residue required firing temperatures of 1200 °C to reach water absorption below 0.5%. The results prove the viability of incorporating porcelain tile polishing residue in sanitary stoneware formulations with up to 2% of porcelain tile polishing residue in replacement of feldspar amount.

#### 5. Acknowledgments

To Luzarte Estrela Ltda – Caruaru -PE industry, for the supply of clays and residue from the porcelain tile polishing. To Arnil Mineração do Nordeste – Parelhas – RN industry, for the supply of feldspar and quartz. The authors acknowledge the financial support from the Brazilian agencies CAPES (Finance Code 001) and Fundação de Amparo à Ciência e Tecnologia de Pernambuco – FACEPE (Grants APQ- 0916-3.03/14).

#### 6. References

- Ramos GA, Pelisser F, Gleize PJP, Bernardin AM, Michel MD. Effect of porcelain tile polishing residue on geopolymer cement. *J Clean Prod.* 2018;191:297-303.
- Matos PR, Prudêncio LR Jr, de Oliveira AL, Pelisser F, Gleize PJP. Use of porcelain polishing residue as a supplementary cementitious material in self-compacting concrete. *Constr Build Mater.* 2018;193:623-30.
- Matos PR, Oliveira AL, Pelisser F, Prudêncio LR Jr. Rheological behavior of Portland cement pastes and self-compacting concretes containing porcelain polishing residue. *Constr Build Mater.* 2018;175:508-18.
- Sanchez E, Ibanez M, García-Ten J, Quereda M, Hutchings I, Xu Y. Porcelain tile microstructure: Implications for polished tile properties. *J Eur Ceram Soc.* 2006;26:2533-40.
- Dondi M, Ercolani G, Guarini G, Melandri C, Raimondo MER, Almendra ER, Cavalcante PT. The role of surface microstructure on the resistance to stains of porcelain stoneware tiles. *J Eur Ceram Soc.* 2005;25:357-65.
- Jacoby P, Pelisser F. Pozzolanic effect of porcelain polishing residue in Portland cement. *J Clean Prod.* 2015;100:84-8.
- Alves H, Freitas M, Melchiades F, Boschi A. Dependence of surface porosity on the polishing depth of porcelain stoneware tiles. *J Eur Ceram Soc.* 2011;31:665-71.
- de’Gennaro R, Graziano SF, Cappelletti P, Colella A, Dondi M, Langella A, et al. Structural concretes with waste-based lightweight aggregates: from landfill to engineered materials. *Environ Sci Technol.* 2009;43:7123-9.
- Shui A, Xi X, Wang Y, Cheng X. Effect of silicon carbide additive on microstructure and properties of porcelain ceramics. *Ceram Int.* 2011;37:1557-62.
- Bittencourt EL, Benincá E. Aspectos superficiais do produto grês polido. *Ceram Ind.* 2002;7:40-6.
- Xi X, Xu L, Shui A, Wang Y, Naito M. Effect of silicon carbide particle size and CaO content on foaming properties during firing and microstructure of porcelain ceramics. *Ceram Int.* 2014;40:12931-8.
- Torres P, Fernandes H, Olhero S, Ferreira J. Incorporation of wastes from granite rock cutting and polishing industries to produce roof tiles. *J Eur Ceram Soc.* 2009;29:23-30.
- Novais RM, Seabra M, Labrincha J. Wood waste incorporation for lightweight porcelain stoneware tiles with tailored thermal conductivity. *J Clean Prod.* 2015;90:66-72.
- Ji R, Zhang Z, He Y, Liu L, Wang X. Synthesis, characterization and modeling of new building insulation material using ceramic polishing waste residue. *Constr Build Mater.* 2015;85:119-26.
- Qi Y, Yue Q, Han S, Yue M, Gao B, Yu H, et al. Preparation and mechanism of ultra-lightweight ceramics produced from sewage sludge. *J Hazard Mater.* 2010;176:76-84.
- Xian Z, Zeng L, Cheng X, Wang H. Effect of polishing waste additive on microstructure and foaming property of porcelain tile and kinetics of sinter-crystallization. *J Therm Anal Calorim.* 2015;122:997-1004.
- Wang H, Chen Z, Liu L, Ji R, Wang X. Synthesis of a foam ceramic based on ceramic tile polishing waste using SiC as foaming agent. *Ceram Int.* 2018;44:10078-86.
- Xiong H, Shui A, Shan Q, Zeng S, Xi X, Du B. Foaming mechanism of polishing porcelain stoneware tile residues via adding C, Al and Si powder. *J Eur Ceram Soc.* 2022;42:1712-21.
- Xiong H, Shui A, Shan Q, Cai M, Xi X, Du B. The cause of foaming in polishing porcelain stoneware tile residues during sintering: Interface corrosion of Silicate-SiC. *J Eur Ceram Soc.* 2022;42:3660-73.
- Sousa IV, Nieves LJJ, Dal-Bó AG, Bernardin AM. Valorization of porcelain tile polishing residue in the production of cellular ceramics. *Cleaner Engineering and Technology.* 2022;6:100381.
- Kırsever D, Toplan HO, Demirkıran AS. Effect of porcelain polishing waste additive on properties and corrosion resistance of ceramic foams produced from zeolite. *Journal of the Australian Ceramic Society.* 2023;59:671-83.
- Bernardin AM, Silva MJ, Riella HG. Characterization of cellular ceramics made by porcelain tile residues. *Mater Sci Eng A.* 2006;437:222-5.
- Rambaldi E, Esposito L, Tucci A, Timellini G. Recycling of polishing porcelain stoneware residues in ceramic tiles. *J Eur Ceram Soc.* 2007;27:3509-15.
- Ke S, Wang Y, Pan Z, Ning C, Zheng S. Recycling of polished tile waste as a main raw material in porcelain tiles. *J Clean Prod.* 2016;115:238-44.
- Capoglu A. A novel low-clay translucent whiteware based on anorthite. *J Eur Ceram Soc.* 2011;31:321-9.
- Marques L, Menezes R, Neves G, Santana L, Lira H, Ferreira H. Re-aproveitamento do resíduo do polimento de porcelanato para utilização em massa cerâmica. *Revista Eletrônica de Materiais e Processos.* 2007;2:34-42.

27. Souza Santos P. *Ciência e tecnologia de argilas*. 2. ed. São Paulo: E. Blücher; 1992.
28. Link M, Bragança S, Bergmann C. Influência da razão SiO<sub>2</sub>/Na<sub>2</sub>O do silicato de sódio na defloculação de suspensões aquosas empregadas na conformação por colagem de barbotinas. *Ceram Ind*. 2013;18:25-8.
29. Morelli AC, Baldo JB. Barbotinas cerâmicas contendo rejeito de vidro soda cal para maturação em baixa temperatura. *Ceram Ind*. 2003;8:42-6.
30. Bernasconi A, Marinoni N, Pavese A, Francescon F, Young K. Feldspar and firing cycle effects on the evolution of sanitary-ware vitreous body. *Ceram Int*. 2014;40:6389-98.
31. Kim K, Kim K, Hwang J. LCD waste glass as a substitute for feldspar in the porcelain sanitary ware production. *Ceram Int*. 2015;41:7097-102.
32. ABNT: Associação Brasileira de Normas Técnicas. ABNT NBR 15097-1: Aparelhos Sanitários de Material Cerâmico - Parte 1: Requisitos e Métodos de Ensaio. Rio de Janeiro: ABNT; 2017.
33. ABNT: Associação Brasileira de Normas Técnicas. ABNT NBR 6225: Materiais refratários conformados- Determinação da variação linear dimensional permanente após aquecimento. Rio de Janeiro: ABNT; 2013.
34. ABNT: Associação Brasileira de Normas Técnicas. ABNT NBR 16661: Materiais refratários densos conformados-Determinação do volume aparente, densidade aparente da parte sólida, porosidade aparente e absorção. Rio de Janeiro: ABNT; 2017.
35. ABNT: Associação Brasileira de Normas Técnicas. ABNT NBR 13818: Placas cerâmicas para revestimento - Especificação e métodos de ensaios. Rio de Janeiro: ABNT; 1997.
36. Lecomte-Nana G, Mokrani A, Tessier-Doyen N, Boussois K, Goure-Doubi H. Texturation of model clay materials using tape casting and freezing. *Ceram Int*. 2013;39:9047-53.
37. Babisk MP, Vidal FWH, Ribeiro WS, Aguiar MS, Gadioli MCB, Vieira MCF. Incorporação de resíduo de quartzitos em cerâmica vermelha. *HOLOS*. 2012;6:169-77.
38. Vieira CMF, Monteiro SN, Barreto CGW, Carvalho EAd, Peiter CC. Substituição de areia de quartzo por finos de gnaise em massa cerâmica para telhas: teste industrial. *Ceramica*. 2008;54:480-6.
39. Norton FH. *Introdução à tecnologia cerâmica*. São Paulo: E. Blucher; 1973.
40. Barba A, Sánchez E, Feliu C, García J, Ginés F, Sanz V, et al. Materias primas para la fabricación de soportes de baldosas cerâmicas. Castellon: ITC; 2002.
41. Menezes RR, Neves GA, Ferreira HC. Argilas plásticas do tipo "Ball Clay". *Revista Eletrônica de Materiais e Processos*. 2014;9:118-24.
42. De Aza AH, Turrillas X, Rodriguez MA, Duran T, Pena P. Time-resolved powder neutron diffraction study of the phase transformation sequence of kaolinite to mullite. *J Eur Ceram Soc*. 2014;34:1409-21.
43. Moraes ÉP, Machado NRCF, Pergher SC. Síntese da zeólita a partir de um caulim brasileiro termicamente ativado. *Acta Sci Technol*. 2003;25:63-9.
44. Silva R, Neves G, Ferreira H, Santana L, Nóbrega A, Menezes R. Uso de dióxido de titânio em massas cerâmicas para grés sanitários. *Ceramica*. 2019;65:1-12.
45. Ngun BK, Mohamad H, Katsumata K, Okada K, Ahmad ZA. Using design of mixture experiments to optimize triaxial ceramic tile compositions incorporating Cambodian clays. *Appl Clay Sci*. 2014;87:97-107.
46. Essakli C, Ider A. Optimization of firing cycle for different porcelain bodies of sanitaryware: the influence of feldspar. *Int J Innov Appl Stud*. 2014;9:115-24.
47. Firat FA, Ercenk E, Yilmaz S. Effect of substitution of basalt for quartz in triaxial porcelain. *J Ceram Process Res*. 2012;13:756-61.